J|A|C|S ARTICLES

Published on Web 08/19/2010

Oxygen Superbases as Polar Binding Pockets in Nonpolar Solvents

Lucie Ducháčková, Aneta Kadlčíková, Martin Kotora, and Jana Roithová*

Department of Organic Chemistry, Charles University in Prague, Hlavova 8, 12843 Prague 2, Czech Republic

Received May 2, 2010; E-mail: roithova@natur.cuni.cz

Abstract: A novel class of chiral superbases derived from the 2,2′-bipyridyl-*N*,*N*′-dioxide skeleton are presented. Combined experimental and theoretical data reveal that their proton affinities are on the order of 1050 kJ mol^{-1}, with protonation occurring at the oxygen atoms in a chelating manner. In the free bases, the oxygen atoms form a strongly polar binding site hidden in a hydrophobic envelope formed by the hydrocarbon backbone of the superbases. This chiral molecular structure can entrap polar intermediates or polarized transition structures and stabilize them in nonpolar solvents. Specifically, this mode of catalysis is shown for the coupling of benzaldehyde and allyltrichlorosilane.

Introduction

The rapidly developing field of organocatalysis provides a whole array of attractive organic molecules that are capable of activating substrates either by specific coordination to their reactive sites[1−4] or by transforming them to more reactive forms.[5−9] Many of the present organocatalysts can be understood as small organic analogues to natural enzymes in that their skeletons are optimized to bind a specific substrate and provide the necessary activation at the correct position. Since activation of the substrate is usually achieved by electrophilic or nucleophilic attack, the catalyst molecules usually bear strongly polar functional groups or the reactive forms may even be charged.[10]

One of the attractive topics in organocatalysis from the mechanistic point of view is enantioselective catalysis with Brønsted bases.[11−15] The reactions are usually initiated by hydrogen abstraction from one of the reactant molecules, and the nucleophile so formed then reacts with the other components in the reaction mixture. For chiral induction during the reaction, it is necessary for the protonated base to remain in the vicinity of the reactants or for the reverse transfer of a proton to the product to proceed enantioselectively. These reactions are usually mediated by very strong bases derived from guanidine[12−15] or even superbases.[16,17]

Scheme 1. Investigated Derivatives of 2,2′-Bipyridyl-*N*,*N*′-dioxide (**1**) (Ph = Phenyl, Me = Methyl, Cy = Cyclohexyl)

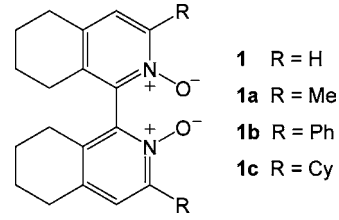

In this work, we investigated the properties and catalytic activity of organocatalysts based on the skeleton of 1,1′-bis(5,6,7,8-tetrahydroisoquinolyl)-*N*,*N*′-dioxide (**1**) (Scheme 1).[18] A key structural feature of **1** is the *N*-oxide groups, which can act together in a chelating manner. Consequently, coordination of **1** with protons or metal cations is expected to involve binding to both *N*-oxide groups. With respect to protonation, this deduction leads to the expectation of a strong basicity of **1** and its derivatives. Hence, as a first step in understanding the coordination features of the title compound, we have determined the experimental as well as theoretical proton affinities of **1a**−**c** and described the electronic structures of the free bases.

Besides the potential applications of derivatives of **1** as Brønsted bases, the arrangement of the *N*-oxide groups also

(1) Rueping, M.; Theissmann, T.; Kuenkel, A.; Koenigs, R. M. *Angew. Chem., Int. Ed.* **2008**, *47*, 6798.
(2) Pihko, P. M. *Angew. Chem., Int. Ed.* **2004**, *43*, 2062.
(3) Taylor, M. S.; Jacobsen, E. N. *Angew. Chem., Int. Ed.* **2006**, *45*, 1520.
(4) Akiyama, T. *Chem. Rev.* **2007**, *107*, 5744, and references therein.
(5) List, B.; Lerner, R. A.; Barbas, C. F., III. *J. Am. Chem. Soc.* **2000**, *122*, 2395.
(6) Notz, W.; List, B. *J. Am. Chem. Soc.* **2000**, *122*, 7386.
(7) Ahrendt, K. A.; Borths, C. J.; MacMillan, D. W. C. *J. Am. Chem. Soc.* **2000**, *122*, 4243.
(8) Diner, P.; Kjærsgaard, A.; Lie, M. A.; Jorgensen, K. A. *Chem.—Eur. J.* **2008**, *14*, 122.
(9) Mukherjee, S.; Yang, J. W.; Hoffmann, S.; List, B. *Chem. Rev.* **2007**, *107*, 5471.
(10) Wong, O. A.; Shi, Y. *Chem. Rev.* **2008**, *108*, 3958, and references therein.
(11) Coles, M. P. *Chem. Commun.* **2009**, 3659.
(12) (a) Shen, J.; Nguyen, T. T.; Goh, Y.-P.; Ye, W.; Fu, X.; Xu, J.; Tan, C.-H. *J. Am. Chem. Soc.* **2006**, *128*, 13692. (b) Terada, M.; Nakano, M.; Ube, H. *J. Am. Chem. Soc.* **2006**, *128*, 16044.
(13) Ube, H.; Shimada, N.; Terada, M. *Angew. Chem., Int. Ed.* **2010**, *49*, 1858.
(14) Leow, D.; Tan, C. H. *Chem.—Asian J.* **2009**, *4*, 488.
(15) Merino, P.; Marques-Lopez, E.; Tejero, T.; Herrera, R. P. *Synthesis* **2010**, 1, and references therein.
(16) Kanazawa, C.; Terada, M. *Chem.—Asian. J.* **2009**, *4*, 1668.
(17) Kondo, Y.; Ueno, M.; Tanaka, Y. *J. Synth. Org. Chem., Jpn.* **2005**, *63*, 453.
(18) (a) Hrdina, R.; Dračínský, M.; Valterová, I.; Hodačová, J.; Císařová, I.; Kotora, M. *Adv. Synth. Catal.* **2008**, *350*, 1449. (b) Kadlčíková, A.; Hrdina, R.; Valterová, I.; Kotora, M. *Adv. Synth. Catal.* **2009**, *351*, 1279.

10.1021/ja103744f

Scheme 2. Mechanistic Dichotomy in the Coupling of Allyltrichlorosilane with Benzaldehyde Catalyzed By (*S*)-**1b**[20]

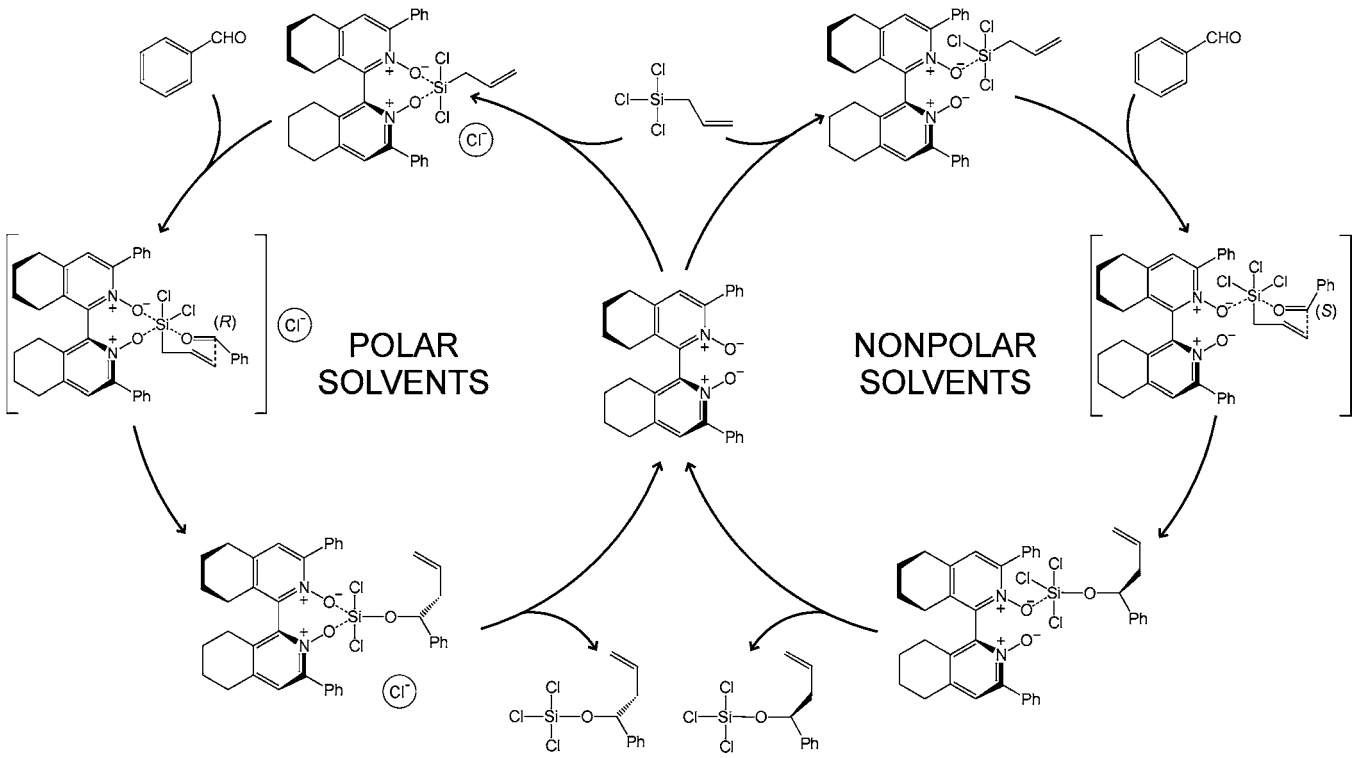

promises their interesting applications as chiral auxiliaries. Currently, the derivatives of **1** have been employed in a Lewis base-type activation of allyl silanes, in which it was assumed that the *N*-oxide groups coordinate to the silicon atom.[19] In particular, these catalysts can be applied in an asymmetric allylation of aromatic as well as α,*β*-unsaturated aldehydes[18] using allyltrichlorosilane as a reagent. Interestingly, the activation of allyltrichlorosilane by the derivatives of **1** very much depends on the solvent used (Scheme 2). Polar solvents (e.g., acetonitrile and dichloromethane) induce formation of the ionized reactant $[\mathbf{1}\cdot SiCl_2(C_3H_5)]^+$, whereas nonpolar solvents (e.g., toluene and chlorobenzene) support the occurrence of the reaction in the neutral state.[20] The change in the mechanism is not only formal but also inverts the chirality of the product alcohols; for example, the reaction between benzaldehyde and $SiCl_3(C_3H_5)$ catalyzed by (*S*)-**1b** in polar solvents proceeds toward (*R*)-1-phenylbut-3-en-1-ol, whereas (*S*)-1-phenylbut-3-en-1-ol is formed in nonpolar solvents.[18] While the reactions in the polar solvents are directed by the interaction of the ionized silicon with the *N*-oxide group(s), the reactions in nonpolar solvents are much more sensitive to the overall electronic structure of the catalyst. Accordingly, larger enantioselectivities also were observed in nonpolar solvents. As our intention was to address the essence of the catalytic activity of derivatives of **1**, we used density functional theory (DFT) to investigate the interaction of **1b** with allyltrichlorosilane and the mechanism of the coupling of the reaction intermediates with benzaldehyde in the nonpolar solvent toluene.

Experimental and Computational Details

The experiments were performed with a TSQ Classic mass spectrometer equipped with an electrospray ionization source and a QOQ configuration of the manifold (Q stands for quadrupole and O for octopole).[21] The proton-bound dimers $(A-H-B)^+$, where A stands for **1a**−**c** and B corresponds to a reference base with known proton affinity [tripropylamine (TPA), tributylamine (TBA), diisopropylethylamine (DIPEA), or 1,8-bis(dimethylamino)naphthalene (DMAN)], were mass-selected by Q1 and collided with xenon at a typical pressure of 7×10^{-5} mbar. The collision energy was adjusted by changing the offset between Q1 and O, while the offset of Q2 was locked to the sum of the offsets of Q1 and O. The zero point of the kinetic energy scale as well as the width of the kinetic energy distribution (fwhm = 1.1 ± 0.1 eV) were determined by means of retarding-potential analysis. The ionic fragments (AH^+ and BH^+) that emerged from the octopole were detected by Q2, and the respective abundances were determined using a Daly-type detector operating in counting mode. The collision energy was changed in steps of 0.25 eV (in the laboratory frame), and 15 scans were accumulated to achieve a good signal-to-noise ratio in the resulting branching ratio. The proton affinities (PAs) given below were derived as averages of three independent measurements.

The complementary calculations of PAs were performed using the DFT method B3LYP[22−25] together with the 6-311+G(2d,p) triple-*ζ* basis set as implemented in the Gaussian 09 suite.[26] Computation of the Hessian matrix was performed for all of the optimized structures at the same level of theory in order to ensure that the structures corresponded to genuine minima as well as to calculate the thermochemical data. In the coupling of allyltrichlorosilane with benzaldehyde catalyzed by **1b**, the interactions between the phenyl substituents of **1b** and the two reactants play an important stabilization role. Therefore, the inclusion of dispersion interactions might be decisive for the

(19) Orito, Y.; Nakajima, M. *Synthesis* **2006**, 1391.
(20) Hrdina, R.; Opekar, F.; Roithová, J.; Kotora, M. *Chem. Commun.* **2009**, 2314.
(21) Ducháčková, L.; Roithová, J. *Chem.—Eur. J.* **2009**, *15*, 13399.
(22) Vosko, S. H.; Wilk, L.; Nusair, M. *Can. J. Phys.* **1980**, *58*, 1200.
(23) Lee, C.; Yang, W.; Parr, R. G. *Phys. Rev. B* **1988**, *37*, 785.
(24) Becke, A. D. *Phys. Rev. A* **1988**, *38*, 3098.
(25) Miehlich, B.; Savin, A.; Stoll, H.; Preuss, H. *Chem. Phys. Lett.* **1989**, *157*, 200.
(26) Frisch, M. J.; et al. *Gaussian 09*, revision A.02; Gaussian, Inc.: Wallingford, CT, 2009.

Table 1. Theoretical and Experimental Proton Affinities (kJ mol^{-1}) of **1a**−**c** and Selected Reference Bases at 0 and 298 K

base[a]	PA^{0K}_{theor}	PA^{298K}_{theor}	PA^{0K}_{exp}	PA^{298K}_{exp}
1a	1036	1042	1047 ± 7[b]	1053 ± 7
1b	1046	1053	1057 ± 7[b]	1064 ± 7
1c	1046	1053	1061 ± 10[b]	1068 ± 10
DMAN	1024	1030		1028.2[c]
TBA	992	998		998.5[c]
DIPEA	994	1001		994.3[c]
TPA	985	991		991.0[c]

[a] For abbreviations of compound names, see the text. [b] The reported values of PA^{0K}_{exp} are averages of three measurements. The error margins are set to the maximum errors evaluated in the individual experiments, as estimated by linear fits over different ranges of the experimental data (for details, see the SI). [c] Data from ref 36.

correct description of the entire system with regard to possible mechanistic implications.[27] With respect to the size of the studied system, we chose to employ DFT with a functional that includes a semiempirical correction for dispersion interaction (DFT-D), namely, the B97D method.[28,29] The geometry optimizations and thermochemistry calculations were performed at the B97D/6-31G* level of theory. The final energies were determined by single-point calculations at the B97D/cc-pVTZ level with corrections for basis-set superposition error (BSSE).[30] It should be noted that the BSSE can be extremely large for the title compounds when small basis sets are used; the errors were on the order of 10 kJ mol^{-1} using the cc-pVTZ basis set. As the last step, solvation energies were determined by single-point calculations using the polarized continuum model at the B97D/cc-pVTZ level.[31] We note in passing that the DFT-D method has been successfully used in the investigation of the reaction mechanism of the same coupling reaction catalyzed by QUINOX, which is an analogous catalyst bearing only a single *N*-oxide site.[32]

Results and Discussion

In order to show the mode of action of the derivatives of **1** in organocatalysis, we first determined their gas-phase proton affinities and electronic structures. The computational results suggest PAs of ~1050 kJ mol^{-1} (Table 1), which are close to those of prototypical nitrogen superbases such as the proton sponge DMAN (PA = 1028 kJ mol^{-1}).[33−35] The large basicities arise from the concentration of negative charge at the oxygen atoms and the fact that both oxygen atoms can coordinate to the proton because of the geometries of **1a**−**c**. Figure 1 shows the electrostatic potentials of the derivative **1c** and its protonated form. The electrostatic potential of the protonated base reveals that the positive charge is delocalized over the whole hydrocarbon backbone of the base.

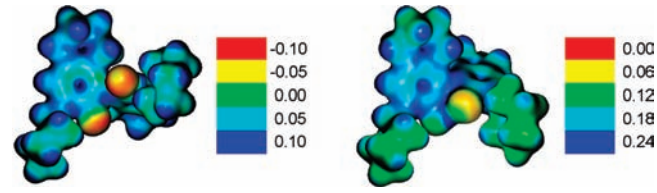

Figure 1. Electrostatic potential maps (in atomic units) for **1c** and its protonated form **1c**·H$^+$ color-coded at the isodensity surface $\rho = 0.02$ e Å^{-3}.

In comparison with those for the bases **1a**−**c**, the proton affinity of the parent compound 2,2′-bipyridyl-*N*,*N*′-dioxide (**2**) is much smaller (1016 kJ mol^{-1}). The effect of the substituents at the 3- and 3′-positions as well as that of the annelated saturated rings can be assessed by means of isodesmic reactions (Scheme 3).[37] Clearly, the inductive effects of the alkyl substituents in the positions ortho to the nitrogen atoms provide the major contributions to the increase in the proton affinity of the derivatives of **1**. The introduction of the methyl groups increases the proton affinity of **2** by 21.5 kJ mol^{-1}, whereas the annelation of the saturated ring results in an increase of only 16.4 kJ mol^{-1}.

Experimentally, the proton affinities of the title compounds were approached using the kinetic method.[38] To this end, we generated mixed proton-bound dimers (A−H−B)$^+$ of **1a**−**c** (A) with several reference bases (B) and investigated the fragmentations of the mass-selected dimers in a triple-quadrupole mass spectrometer. The ratio of the abundances of the fragments AH$^+$ and BH$^+$ upon collisional activation reflects the ratio of dissociation rates of (A−H−B)$^+$ to AH$^+$ and BH$^+$, respectively (eq 1; GB = gas-phase basicity, PA = proton affinity, T_{eff} = effective temperature reflecting the internal energy of the fragmenting ion).

$$\ln\left(\frac{I_{AH^+}}{I_{BH^+}}\right) \approx \ln\left(\frac{k_A}{k_B}\right) \approx \frac{GB_A - GB_B}{RT_{eff}} \approx \frac{PA_A - PA_B}{RT_{eff}} \quad (1)$$

The rather large proton affinities of the title compounds predicted by theory limited our selection of reference bases to some of the most basic nitrogen compounds available, namely, proton sponge (DMAN), Hünig base (DIPEA), TBA, and TPA. The significantly diverse structures of the title compounds and the reference bases most probably led to different entropic changes upon their protonation. Thus, the conversion from gas-phase basicities (determined from Gibbs free energies) and proton affinities (determined from enthalpies) was not as straightforward as suggested by eq 1, so we used the extended kinetic method (Figure 2).[39,40]

(27) Hobza, P.; Müller-Dethlefs, K. *Non-covalent Interactions: Theory and Experiment*; RSC Theoretical and Computational Chemistry Series, No. 2; Royal Society of Chemistry: Cambridge, U.K., 2010.
(28) Grimme, S. *J. Comput. Chem.* **2006**, *27*, 1787.
(29) Pevarati, R.; Baldridge, K. K. *J. Chem. Theory Comput.* **2008**, *4*, 2030.
(30) Boys, S. F.; Bernardi, F. *Mol. Phys.* **1970**, *19*, 553.
(31) Tomasi, J.; Mennucci, B.; Cammi, R. *Chem. Rev.* **2005**, *105*, 2999.
(32) Malkov, A. V.; Ramírez-López, P.; Biedermannová, L.; Rulíšek, L.; Dufková, L.; Kotora, M.; Zhu, F.; Kočovský, P. *J. Am. Chem. Soc.* **2008**, *130*, 5341.
(33) Roithová, J.; Schröder, D.; Míšek, J.; Stará, I.; Starý, I. *J. Mass Spectrom.* **2007**, *42*, 1233.
(34) (a) Eckert-Maksic, M.; Glasovac, Z.; Troselj, P.; Kutt, A.; Rodima, T.; Koppel, I.; Koppel, I. A. *Eur. J. Org. Chem.* **2008**, 5176. (b) Coles, M. P.; Aragon-Saez, P. J.; Oakley, S. H.; Hitchcock, P. B.; Davidson, M. G.; Maksic, Z. B.; Vianello, R.; Leito, I.; Kaljurand, I.; Apperley, D. C. *J. Am. Chem. Soc.* **2009**, *131*, 16858.
(35) (a) Verkade, J. G. *Top. Curr. Chem.* **2003**, *223*, 1. (b) Kolomeitsev, A. A.; Koppel, I. A.; Rodima, T.; Barten, J.; Lork, E.; Roschenthaler, G. V.; Kaljurand, I.; Kutt, A.; Koppel, I.; Maemets, V.; Leito, I. *J. Am. Chem. Soc.* **2005**, *127*, 17656. (c) Tailefer, M.; Rahier, N.; Hameau, A.; Volle, J. N. *Chem. Commun.* **2006**, 3238.
(36) Hunter, E. P.; Lias, S. G. *J. Phys. Chem. Ref. Data* **1998**, *27*, 413.
(37) Exner, O. *J. Phys. Org. Chem.* **1999**, *12*, 265.
(38) (a) Cooks, R. G.; Wong, P. S. H. *Acc. Chem. Res.* **1998**, *31*, 379. (b) Cooks, R. G.; Koskinen, J. T.; Thomas, P. D. *J. Mass Spectrom.* **1999**, *34*, 85.
(39) Drahos, L.; Vekey, K. *J. Mass Spectrom.* **2003**, *38*, 1025.
(40) For insightful essays about the performance and inherent problems of the kinetic method, see: (a) Bouchoux, G.; Sablier, M.; Berruyer-Penaud, F. *J. Mass Spectrom.* **2004**, *39*, 986. (b) Wesdemiotis, C. *J. Mass Spectrom.* **2004**, *39*, 998. (c) Ervin, K. M.; Armentrout, P. B. *J. Mass Spectrom.* **2004**, *39*, 1004. (d) Drahos, L.; Peltz, C.; Vekey, K. *J. Mass Spectrom.* **2004**, *39*, 1016.

Scheme 3. Isodesmic Reactions Used To Evaluate the Effect of the Substituents on the Basicity Of **2**

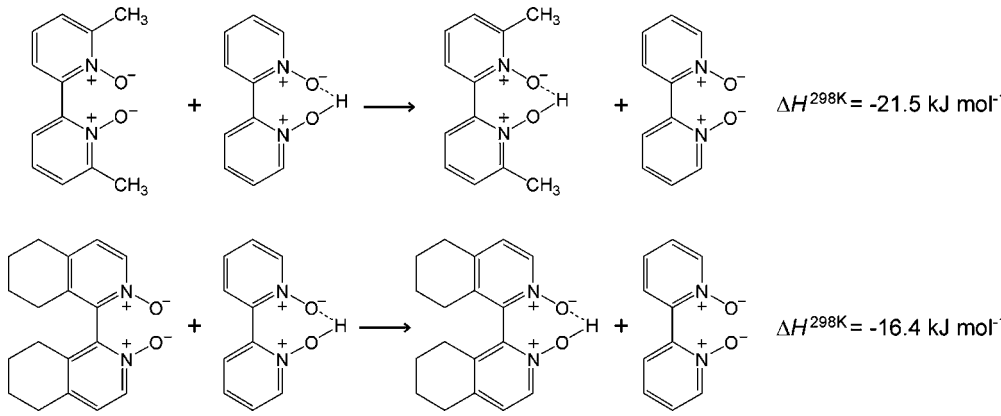

The effect of entropy on the gas-phase basicity depends on the temperature and can be approached experimentally by performing the dissociation experiment with $(A-H-B)^+$ at different collision energies. Figure 2a shows the determination of the so-called apparent gas-phase basicity (GB_{app}) of **1b** at collision energies of 2.4 and 3.6 eV, respectively. At a given collision energy, the intersection of the linear fit of $\ln(I_{\mathbf{1b}H+}/I_{BH+})$ as a function of PA_B (B = DMAN, DIPEA, TBA, TPA) with the horizontal axis reveals GB_{app}(**1b**) and the slope of the linear fit is equal to $(RT_{eff})^{-1}$ (see eq 1).[41] The value of GB_{app}(**1b**) does not correspond to any observable thermodynamic property, as it contains entropy contributions from all of the processes involved in its determination. In an ideal case, however, the linear extrapolation of the dependence of GB_{app} to the effective temperature $T_{eff} = 0$ K would lead to the elimination of all entropy effects and directly yield the proton affinity of the studied compound at 0 K. Such a treatment of our experimental data from three independent measurements gave the proton affinities, which are listed in Table 1 [for all of the experimental data and the detailed evaluation of PA_{exp}^{0K} values, see the Supporting Information (SI)]. With respect to the large experimental errors in the determination of the entropies,[40] the final proton affinities were obtained as a sum of PA_{exp}^{0K} and the theoretical correction for the temperature effect ($PA_{theor}^{298K} - PA_{theor}^{0K}$) (Table 1).[42]

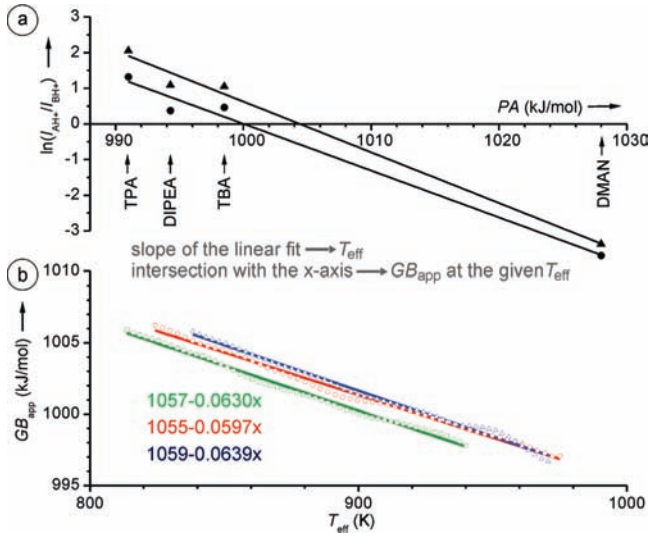

Figure 2. Determination of the proton affinity of **1b** using the extended kinetic method. (a) Determination of the gas-phase basicity of **1b** at collision energies of 2.4 (▲) and 3.6 eV (●) by linear fits of the dependences of $\ln(I_{AH+}/I_{BH+})$ as a function of the PA of the reference base B. The intersection of a given linear fit with the horizontal axis gives GB_{app}(**1b**). The effective temperature corresponding to a given collision energy is determined from the slope of the linear fit. (b) Dependence of GB_{app}(**1b**) on the effective temperature (results of three measurements). The extrapolations of the linear fits of the data obtained in the E_{CM} range 2.0−4.4 eV to $T_{eff} = 0$ K gives the estimates of PA_{exp}^{0K} (the linear fits for the three measurements are given by their equations in the respective colors).

The experimental proton affinities of the studied derivatives of **1** exceed 1050 kJ mol^{-1}, and the results thus fully support the calculations and demonstrate that the derivatives of **1** are exceptionally strong oxygen bases whose basicities exceed even that of DMAN. We note in passing that in the collision experiments, which were performed at rather high effective temperatures (∼900 K), DMAN showed larger basicity than any of the derivatives of **1**. The seeming conflict can be easily explained by considering entropy effects: If we calculate the basicity differences (determined from $\Delta\Delta G$) between DMAN and **1a** at 298, 1000, and 2000 K, we obtain differences of −12, −3, and +5 kJ/mol, respectively. Thus, DMAN is more basic than the derivatives of **1** at large internal energies, at which we performed our experiments. This result can be attributed to the changes in geometry upon protonation of **1** and locking of the dihedral angle between the two tetrahydroisoquinoline rings.

The most basic organic oxygen bases known to date are based on pyrone-like structures, whose large basicity is a result of delocalization of the charge over the aromatic backbone (Scheme 4).[43,44] The charge of the incoming proton is either delocalized over the aromatic ring (structure A) or transferred to the nitrogen substituents in the base (structure B). It should be also noted that all of these oxygen superbases have been studied only theoretically. Apart from these neutral bases, there is a series of anionic oxygen bases (e.g., alkoxides) whose extreme basicity

(41) (a) Drahos, L.; Vekey, K. *J. Mass Spectrom.* **1999**, *34*, 79. (b) Ervin, K. M. *Int. J. Mass Spectrom.* **2000**, *195/196*, 271. (c) Laskin, J.; Futrell, J. *J. Phys. Chem. A* **2000**, *104*, 8829. (d) Armentrout, P. B. *J. Am. Soc. Mass Spectrom.* **2000**, *11*, 371.

(42) We also probed the collisional experiments using argon as a collision gas and using an ion-trap instrument in order to obtain data at different effective temperatures. In contrast to the exclusive dissociations of the proton-bound dimers to the protonated bases obtained in the experiments with xenon (see the SI for the spectra), the experiments with argon and in the ion trap also led to other dissociation channels, such as oxygen transfers from the *N*-oxide bases, so we did not include those data here.

(43) Suarez, D.; Menendez, J. A.; Fuente, E.; Montes-Moran, M. A. *Angew. Chem., Int. Ed.* **2000**, *39*, 1320.

(44) Despotovic, I.; Maksic, Z. B.; Vianello, R. *Eur. J. Org. Chem.* **2007**, 3402.

Scheme 4. Theoretically Predicted Oxygen Superbases A and B (Only the Most Basic Representatives of the Corresponding Classes of Compounds Are Shown) and Experimentally Investigated Superbase C[a]

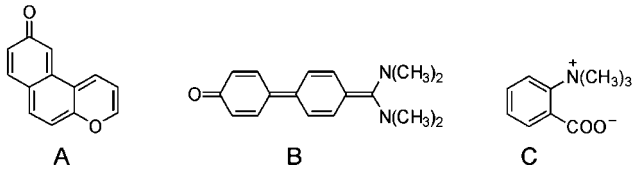

[a] The proton affinities amount to $PA_A = 1054$ kJ mol^{-1} [43] and $PA_B = 1138$ kJ mol^{-1},[44] and the gas-phase basicity of C is 1028 kJ mol^{-1}.[46]

is a result of neutralization of their negative charge.[45] A similar situation is also found for zwitterionic compounds such as species C in Scheme 4, where the negatively charged group is protonated, resulting in localization of the positive charge on the ammonium group.[46] The experimental gas-phase basicity of this zwitterion amounts to 1028 kJ mol^{-1}, and it was also determined by the kinetic method as applied here. The derivatives **1a**−**c** of 2,2′-bipyridyl-*N*,*N*′-dioxide are derived from a family of pyridine *N*-oxide compounds,[47] and their special backbone arrangement makes them a new class of chiral oxygen superbases that can easily be synthetically prepared and used in catalysis.[18,48]

Having determined the exceptionally large basicities of the derivatives of **1**, which are associated with strongly polar sites constituted by two *N*-oxide functions, we then investigated the mode of action of one of the catalysts, **1b**, in allylations of benzaldehyde proceeding in toluene, as mentioned in the Introduction.

The reaction in polar solvents proceeds in the ionized state,[20] in which the catalyst coordinates to the silicon atom of the allyldichlorosilicenium ion. According to the previously suggested mechanism, the oxygen atom of benzaldehyde coordinates to the silicon atom of the cationic complex, and the C−C coupling can proceed via a six-membered transition structure (Scheme 1).[32] An analogous mechanism in the neutral state would involve either seven-coordinate silicon, which appears to be rather improbable, or coordination to silicon by only one of the oxygen atoms of the organocatalyst (Scheme 1). However, both scenarios impose large steric demands on the approach of benzaldehyde to the primary complex of **1b** and allyltrichlorosilane. On the other hand, however, **1b** is a very efficient catalyst, and the coupling proceeds faster than with other catalysts bearing a less sterically demanding structure.[49] In order to understand the special catalytic activity of **1b**, we addressed its mode of action toward allyltrichlorosilane and benzaldehyde in toluene using DFT calculations with an empirical correction for the dispersion energy (i.e., we used the B97D functional).

Table 2. B97D/cc-pVTZ[a] Energetics of Intermediates and Transition States (kJ mol^{-1}) for the Formation of (*S*)- and (*R*)-4-Phenylbut-1-en-4-oxytrichlorosilane Catalyzed by (*S*)-**1b**[a]

	gas-phase			in toluene	
	ΔH^{0K} [b]	ΔH^{298K} [b]	ΔG^{298K} [c]	ΔH^{298K} [b]	ΔG^{298K} [c]
TS1	82			74	137
TS2	47			43	108
3a	14			5	59
3b	−41			−34	13
3c	−40			−32	14
(*S*)-TS3_a	39	36	164	34	162
(*S*)-TS3_b	55	52	179	48	175
(*R*)-TS3_a	35	33	162	30	160
(*R*)-TS3_b	58	56	182	53	179
(*S*)-TS4_a	9	8	125	12	128
(*S*)-TS4_b	8	7	126	13	131
(*S*)-TS4_c	10	9	132	13	137
(*R*)-TS4_a	3	2	119	12	128
(*R*)-TS4_b	11	10	126	15	130

[a] Geometry optimizations and thermochemistry calculations were performed at the B97D/6-31G* level of theory. The total energies were refined by single-point calculations including the BSSE correction, and the solvation free energies were obtained by single-point PCM calculations, both at the B97D/cc-pVTZ level. [b] Energies are given relative to the sum of the enthalpies of the reactants (for more details, see the SI). [c] Energies are given relative to the sum of the Gibbs free energies of the reactants (see the SI).

According to our computational investigations of complexes of **1b** with allyltrichlorosilane, the coordination of **1b** via the oxygen atom(s) to the silicon atom of allyltrichlorosilane is endothermic (complex **3a**, Figure 3). In contrast, the coordination of **1b** via the hydrogen atoms of the allyl group is energetically favored (complexes **3b** and **3c**). These results suggest that the oxygen atoms of **1b** do not interact directly with the sterically hindered silicon atom of allyltrichlorosilane; instead, the catalyst **1b** forms a polar pocket that interacts with the whole polarized backbone of allyltrichlorosilane.

The noncatalyzed coupling between benzaldehyde and allyltrichlorosilane in toluene proceeds via an energy barrier of 74 kJ mol^{-1} (TS1 in Table 2 and Figure 4).[32,50] We have further considered possible catalysis by a chloride ion, which might be present in the reaction mixture as a result of partial

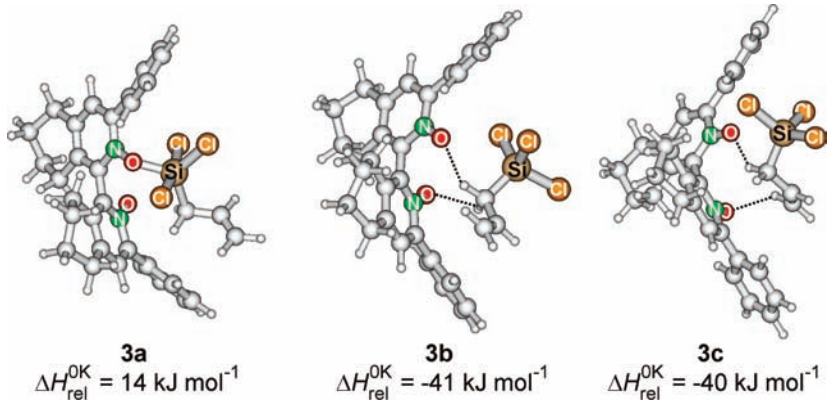

Figure 3. Different modes of coordination between **1b** and allyltrichlorosilane. Energies refer to the sum of the energies of **1b** and $(C_3H_5)SiCl_3$ at 0 K in the gas phase.

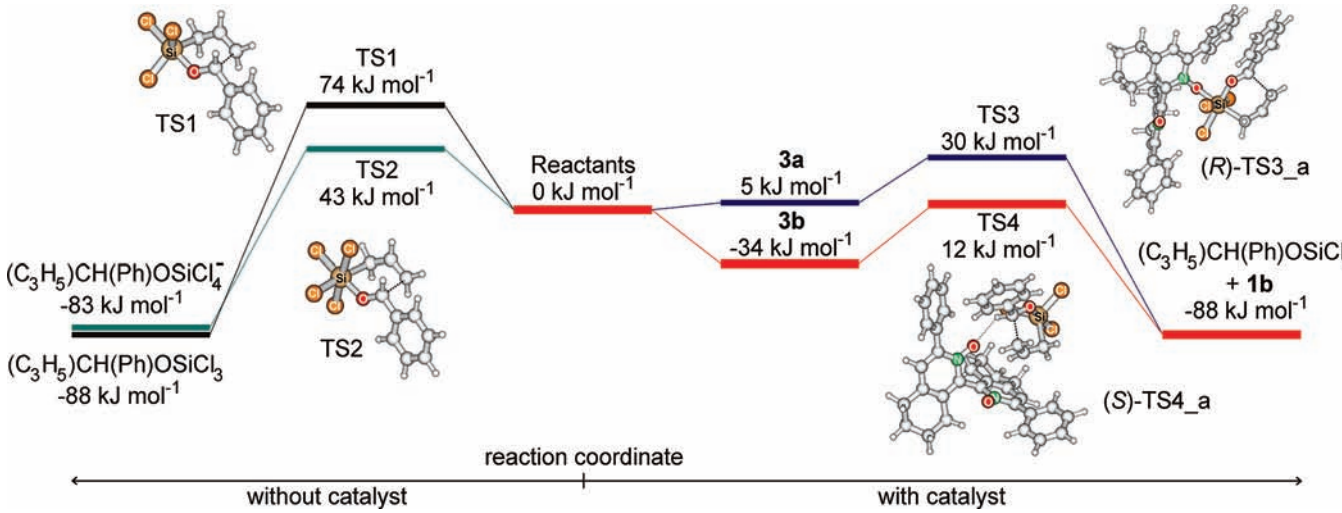

Figure 4. B97D/cc-pVTZ//B97D/6-31G* potential energy surface for the coupling of allyltrichlorosilane ($C_3H_5SiCl_3$) with benzaldehyde (PhCHO) in toluene. The structures show the optimized geometries of the transition states. Energies are given relative to the sum of the enthalpies of the reactants at 298 K in toluene (for details, see the SI). It should be noted that reactants are $C_3H_5SiCl_3$ + PhCHO for the uncatalyzed reaction (black), $C_3H_5SiCl_4^-$ + PhCHO for the anionic reaction (green), and $C_3H_5SiCl_3$ + PhCHO + (*S*)-**1b** for the organocatalytic reaction (blue and red).

Scheme 5. Hydrolysis of Allyltrichlorosilane and Removal of HCl from the Reaction Mixture

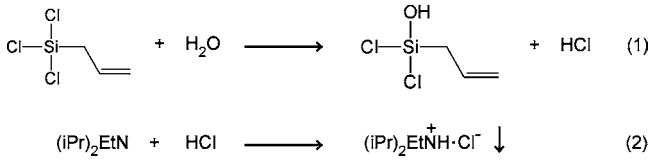

hydrolysis of allyltrichlorosilane with traces of moisture (Scheme 5). The coordination of a chloro ligand to the silicon decreases the reaction barrier by ~30 kJ mol^{-1} (TS2). Such a reaction represents an undesired pathway, however, because it leads to a racemic mixture of products. It has been reported that the addition of Hünig base to the reaction mixture is essential for the high enantiomeric excess obtained in the reaction.[51,52] According to the above results, we hence suggest that the role of the added base is to generate the ammonium chloride salt, which brings two effects at once. First, it removes from the solution protons that would otherwise be bound to the strongly basic catalyst **1b** and thus deactivate it for the coupling step. Second, the precipitation of ammonium chloride from the toluene solution removes the free chloride ions from the reaction mixture, which would otherwise promote the nonenantioselective coupling (Scheme 5).

In the next step, we investigated the effect of the catalyst **1b** on the barrier height for the coupling reaction. First, the activation of allyltrichlorosilane by coordination of the catalyst via the oxygen atom was considered. Two types of transition structures were localized. The lower-energy pathways proceed via the transition structures (*S*)-TS3_a and (*R*)-TS3_a, which are stabilized by the stacking interaction of the benzene rings of the catalyst and benzaldehyde [Figure 5; the prefixes (*S*) and (*R*) denote the chirality of the product formed].[53] The corresponding reaction barriers are slightly lower than that for the reaction catalyzed by chloride and amount to 34 kJ mol^{-1} for the formation of the *S* product and 30 kJ mol^{-1} for the formation of the *R* product (blue pathway in Figure 4). With inclusion of the entropy effects (see the Gibbs free energies in Table 2), the reaction pathways proceeding via the two TS3_a structures are much less favored than the reaction catalyzed by chloride; moreover, they are less favored than the noncatalyzed reaction. The geometries of the transition structures (*S*)-TS3_b and (*R*)-TS3_b do not suggest any major stabilization by the backbone of the catalyst; accordingly, they lie more than 10 kJ mol^{-1} higher in energy than both of the TS3_a structures and therefore were not considered further.

As an alternative, different reaction pathways were discovered for the approach of benzaldehyde to the complexes derived from **3b** and **3c** (red pathway in Figure 4). Such interactions lead to transition structures that are very low in energy relative to the separated reactants (Figure 5 and Table 2). The transition structures are stabilized by a number of interactions within the polar pocket formed by the catalyst

(45) (a) Arnett, E. M.; Moe, K. D. *J. Am. Chem. Soc.* **1991**, *113*, 7288. (b) Majumdar, T. K.; Clairet, F.; Tabet, J.-C.; Cooks, R. G. *J. Am. Chem. Soc.* **1992**, *114*, 2897.
(46) Strittmatter, E. F.; Wong, R. L.; Williams, E. R. *J. Am. Chem. Soc.* **2000**, *122*, 1247.
(47) (a) Makowski, M.; Tomaszewski, R.; Kozak, A.; Chmurzynski, L. *J. Phys. Chem. A* **2001**, *105*, 7381. (b) Berdys, J.; Makowski, M.; Makowska, M.; Puszko, A.; Chmurzynski, L. *J. Phys. Chem. A* **2003**, *107*, 6293.
(48) Formally, the diatomic neutral alkaline-earth oxides (particularly CaO, SrO, and BaO) are the strongest oxygen superbases known, but they are not comparable with the organocatalysts studied here.
(49) The allylation of benzaldehyde with allyltrichlorosilane catalyzed by **1b** (0.1 mol %) in chlorobenzene at −40 °C gives 100% yield with 80% ee in 1 h.[18a] For comparison, the same reaction catalyzed by QUINOX [1-(2-methoxynaphth-1-yl)isoquinoline *N*-oxide) (5 mol %) in CH_2Cl_2 at −40 °C gives 68% yield with 87% ee in 12 h, and only <5% yield is observed after 12 h when the reaction is conducted at −40 °C in toluene.[32]
(50) Sakata, K.; Fujimoto, H. *Organometallics* **2010**, *29*, 1004.
(51) Nakajima, M.; Saito, M.; Shiro, M.; Hashimoto, S. *J. Am. Chem. Soc.* **1998**, *120*, 6419.
(52) The allylation of benzaldehyde with allyltrichlorosilane catalyzed by (*R*)-**1b** (10 mol %) in PhCl (−40 °C, 1 h) without Hünig base (DIPEA) yielded only racemic product (50%). No asymmetric induction was observed.
(53) Lee, E. C.; Kim, D.; Jurečka, P.; Tarakeshwar, P.; Hobza, P.; Kim, K. S. *J. Phys. Chem. A* **2007**, *111*, 3446.

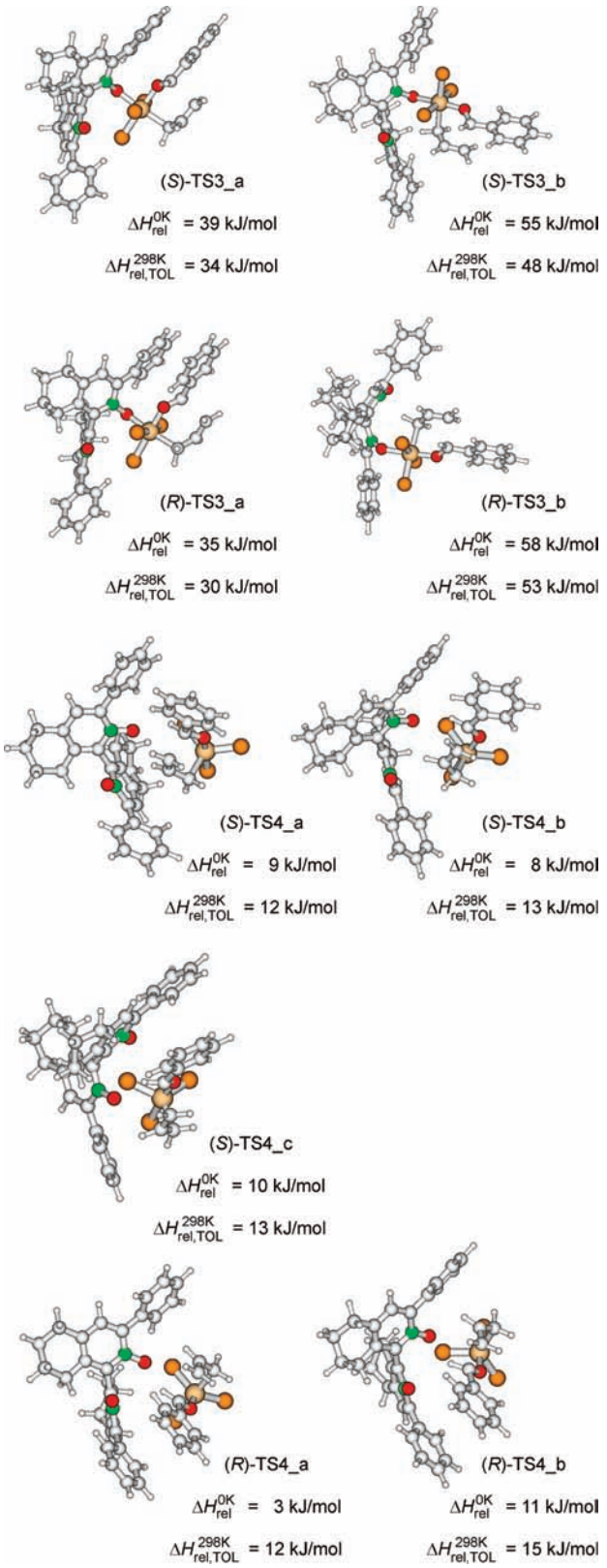

Figure 5. Transition structures for the reaction of allyltrichlorosilane with benzaldehyde catalyzed by (*S*)-**1b**. The energies refer to the gas phase at 0 K and to toluene at 298 K and are given relative to the separated reactants.

1b. In addition to the dipole interactions between the *N*-oxide groups and various C−H bonds, the structures are also stabilized by dispersion interactions between the phenyl substituents of **1b** and the reactants as well as dipole interactions between the chlorine atoms and the C−H bonds of the annelated saturated rings of **1b**. We localized several transition structures that lie very close in energy. The lowest energy barriers for the formation of the *S* and *R* products both amount to 12 kJ mol^{-1}. Also, when entropic factors are taken into account, the "pocket" mechanism remains clearly favored over the mechanism proceeding via six-coordinate silicon as well as over the noncatalyzed coupling.

As far as the enantioselectivity of the coupling is concerned, our results do not reproduce the experimentally observed preference for the formation of the *S* product. We are aware of the limitations of the theoretical approach chosen, and therefore, we do not dwell upon the small energy differences between (*S*)- and (*R*)-TS4 but rather point to the large structural and energetic differences between TS3 and TS4. The intention is thus to show the modes of action of the catalysts derived from **1** rather than to deliver ultimately exact energy barriers. We note in passing that for the correct description of the chiral preferences in the reaction, correlated ab initio calculations with BSSE corrections would have to be applied; however, this would be extremely computationally demanding, particularly because in a strict sense this level would also be required in the geometry optimizations. Moreover, our inclusion of solvation as an a posteriori correction is a fair compromise but has its limits.

In a more general sense, we can say that the catalyst **1b** behaves similar to an enzyme in that it provides a well-structured, strongly polar pocket for stabilization of a polarized molecular structure in otherwise nonpolar environment. However, it should be noted that in comparison to most enzymes, the pocket and the medium have reversed phases in **1b**. Figure 6 illustrates the mode of action of **1b** in the coupling reaction and the role of the polar pocket in particular. In the most stable conformation of **1b**, the *N*-oxide binding sites point to the opposite sides of the plane tentatively formed by the phenyl substituents. Notably, this conformation is operative in the TS3-type transition structures. The "pocket" conformation of **1b** lies 3 kJ mol^{-1} higher in energy, and the illustration shows a putative interaction mode of **1b** with the transition structure TS1 for the coupling reaction.

Such a mode of reactivity can be very promising for other electrocyclic reactions proceeding in nonpolar solvents, such as Diels−Alder reactions.[15] In principle, many axially chiral guanidine bases currently used for an increasing number of organocatalytic reactions have a similar structure. They are often derived from 1,1′-biaryls that are connected to guanidine via methylene bridges at the 2 and 2′ positions and have large aromatic substituents at the 3 and 3′ positions. Thus, these bases may in fact form similar chiral pockets in the active steps of catalysis of a variety of reactions with high enantioselectivities. The concept of chiral pockets itself might thus have implications beyond the range of the title compounds, and we will explore this aspect in forthcoming work.

Conclusions

Using a mass-spectrometric kinetic method and theoretical calculations, we have studied a new class of organic chiral oxygen superbases whose proton affinities exceed 1050 kJ mol^{-1}. In contrast to other theoretically predicted oxygen superbases, the basicity of **1a**−**c** stems from a strongly polar binding site consisting of two *N*-oxide functions. The positive charge formed upon protonation is mostly stabilized by the

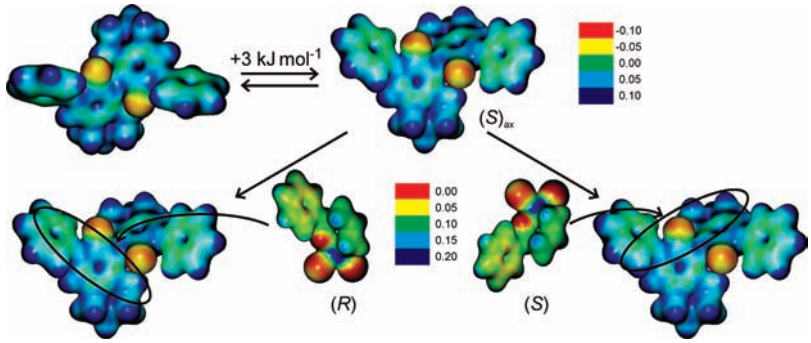

Figure 6. Illustration of the "polar pocket" stabilization of the transition structure for the coupling of allyltrichlorosilane with benzaldehyde by (*S*)-**1b**. Molecules are depicted by their electrostatic potential (in atomic units) color-coded at the isodensity surface $\rho = 0.02$ e Å^{-3}. The different scales for TS1 and (*S*)-**1b** should be noted. The reaction enthalpy refers to 298 K and toluene solvation.

inductive effect of the hydrocarbon backbone of the superbases. The congested and very polar molecular structure of these compounds provides a specific chiral binding pocket that can entrap polar intermediates or polarized transition structures and hence stabilize them in nonpolar environments. In particular, we have investigated the coupling between allyltrichlorosilane and benzaldehyde catalyzed by **1b** in the *nonpolar* medium toluene. By analogy to the previously described catalysis by *N*,*N*-dimethylformamide or the structurally related catalyst QUINOX, we have found reaction pathways in which allyltrichlorosilane is coordinated to one of the *N*-oxide functions of **1b**. In addition, however, we have discovered an alternative, energetically favored mechanism that is based on stabilization of the transition structure by dipole and weak interactions within the polar pocket of the catalyst. This special catalytic mode may offer new perspectives for reactions that proceed via polarized transition structures and are performed in nonpolar solvents.

Acknowledgment. Support by the Ministry of Education of the Czech Republic (MSM0021620857) and the Charles University Grant Agency (259029) is acknowledged.

Supporting Information Available: Detailed evaluation of the proton affinities, details of the theoretical approach chosen, total energies, optimized geometries, and complete ref 26. This material is available free of charge via the Internet at http://pubs.acs.org.

JA103744F